Probability distributions of surface gravity waves during spectral changes

By HERVÉ SOCQUET-JUGLARD[1], KRISTIAN DYSTHE[1], KARSTEN TRULSEN[2], HARALD E. KROGSTAD[3] AND JINGDONG LIU[3]

[1]Department of Mathematics, University of Bergen,

[2]Department of Mathematics, University of Oslo,

[3]Department of Mathematics, NTNU, Trondheim,

Q1

Simulations have been performed with a fairly narrow band numerical gravity wave model (higher-order NLS type) and a computational domain of dimensions 128×128 typical wavelengths. The simulations are initiated with $\sim 6 \times 10^4$ Fourier modes corresponding to truncated JONSWAP spectra and different angular distributions giving both short- and long-crested waves. A development of the spectra on the so-called Benjamin–Feir timescale is seen, similar to the one reported by Dysthe *et al.* (*J. Fluid Mech.* vol. 478, 2003, P. 1). The probability distributions of surface elevation and crest height are found to fit theoretical distributions found by Tayfun (*J. Geophys. Res.* vol. 85, 1980, p. 1548) very well for elevations up to four standard deviations (for realistic angular spectral distributions). Moreover, in this range of the distributions, the influence of the spectral evolution seems insignificant. For the extreme parts of the distributions a significant correlation with the spectral change can be seen for very long-crested waves. For this case we find that the density of large waves increases during spectral change, in agreement with a recent experimental study by Onorato *et al.* (*J. Fluid Mech.* 2004 submitted).

1. Introduction

In recent years there has been a growing interest in so-called *freak* or *rogue* waves (see e.g. the proceedings from the workshop Rogue Wave 2000, IFREMER, Olagnon & Athanassoulis 2000; and also Kharif & Pelinovsky 2004). In coastal waters the occurrence of extreme waves can often be explained by focusing (or caustics) due to refraction by bottom topography or strong current gradients. Well-documented in that respect are the giant waves frequently reported in the Agulhas Current off the eastern coast of South Africa.

Also, on the open deep ocean there seem to be indications of extreme events that are not plausibly explained by the current state-of-the-art wave statistics (Haver & Andersen 2000) (in fact, they suggest as a definition of a freak wave event, that it is not plausibly explained by second-order wave models). A number of physical effects have been suggested that could focus wave energy to produce large waves. In order to work, however, they all seem to need some special preparation or coherence (Dysthe 2000). It is difficult to envision how these conditions would occur spontaneously during a storm on the open ocean. A possible exception is the conjecture that freak waves are associated with a form of spectral instability. For two-dimensional waves

both theory and simulations (Onorato *et al.* 2000; Mori & Yasuda 2000; Janssen 2003), and experiments in a waveflume (Onorato *et al.* 2004) have given results in support of this idea. Testing this conjecture in the three-dimensional case is a central theme of the present paper.

It is well-known that a uniform train of surface gravity waves is unstable to the so-called modulational, or Benjamin–Feir (BF) instability (Lighthill 1965, 1967; Benjamin & Feir 1967; Zakharov 1967; Whitham 1967). The instability takes place on the timescale $(s^2\omega)^{-1}$, where s and ω are the wave steepness and frequency, respectively. The stability of nearly Gaussian random wave fields of narrow bandwidth around a peak frequency ω_p was considered by Alber & Saffman (1978), Alber (1978), and Crawford, Saffman & Yuen (1980). Their results were based on the nonlinear Schrödinger (NLS) equation and suggested that narrow-band spectra may evolve on the BF timescale $(s^2\omega_p)^{-1}$, provided that the relative spectral width $\Delta\omega/\omega_p$ does not exceed the steepness. For wider spectra, change should only occur on the much longer Hasselmann timescale $(s^4\omega_p)^{-1}$ (Hasselmann 1962; Crawford *et al.* 1980).

In a recent paper (Dysthe *et al.* 2003) we investigated the stability of moderately narrow wave spectra by numerical simulations. Starting from a bell-shaped initial spectrum, we find that regardless of the initial spectral width, the spectra evolve on the BF timescale from an initial symmetrical form into a skewed shape with a downshift of the peak frequency. In three dimensions, the angularly integrated spectrum shows an evolution towards a power-law behaviour ω^{-4} on the high-frequency side.

In two dimensions similar results have been obtained by Mori & Yasuda (2000) using the full Euler equations, and by Janssen (2003) using the Zakharov integral equation. In three dimensions Onorato *et al.* (2002), using the full Euler equations, demonstrated that a spectral evolution and the power-law behaviour ω^{-4} occur for a wide spectral range. In two-dimensional simulations it was also found by Onorato *et al.* (2000) and by Mori & Yasuda (2000) that large waves appeared to be associated with rapid spectral development due to the modulational instability.

Recently Onorato *et al.* (2004) have performed experiments in a long wave flume with a paddle-generated JONSWAP spectrum, and demonstrated an increase in the density of rogue waves associated with spectral instability. They also compared the results with corresponding numerical simulations using a higher-order NLS-type equation, getting quite good agreement.

In the present paper we first investigate the spectral development of the surface starting from an initial condition with random spectral amplitudes chosen from truncated JONSWAP spectra and various directional distributions. The higher-order NLS-type equations used were discussed in Dysthe (1979), Trulsen & Dysthe (1996), and Trulsen *et al.* (2000). The results are similar to those reported in Dysthe *et al.* (2003), and show that in the present case also a spectral evolution takes place on the BF timescale. The spectral changes are more pronounced when the initial spectral width decreases.

The main part of the paper is concerned with the statistical distributions of surface elevation and crest height, and the influence of spectral change. In the narrow-band expansion used in our model it is found that the first harmonic term has a Gaussian distribution to a good approximation for surface elevations up to four standard deviations (for short-crested waves). Tayfun (1980) derived a second-order correction to the Gaussian distribution of the surface elevation for the narrow-band case, starting from the hypothesis that the first harmonic is Gaussian. It is then not surprising that the higher-order reconstructions of the surface have distributions of elevation and

crest height that are approximated well by the Tayfun distributions. What did surprise us is the fact that for short-crested waves they seem to fit our simulated data up to five standard deviations!

An important question is whether the rather fast spectral evolution that we see during the initial part of our simulations changes the statistical properties of the simulated surface. In the computational domain (128×128 typical wavelengths) we have roughly $10\,000$ waves at any instant of time, and it is therefore possible to estimate whether the distributions of surface elevation and crest height change with the wave spectrum. For the bulk of the waves, the distributions seem to be virtually independent of the spectral change. For the more extreme waves, we find a dependence. It is hardly noticeable in the short-crested case. For the long-crested case, however, the dependence is clearly seen. Our findings for this case appear to be in good agreement with the results of the experiments of Onorato *et al.* (2004).

2. The simulation model

The higher-order NLS-type equations used in the present simulations have been discussed in Dysthe (1979), Trulsen & Dysthe (1996) and Trulsen *et al.* (2000), and are not reproduced here. The wave field is assumed to have a moderately narrow spectral width, so that the surface elevation, η, is represented as

$$\eta = \bar{\eta} + \tfrac{1}{2}(B e^{i\theta} + B_2 e^{2i\theta} + B_3 e^{3i\theta} \cdots + \text{c.c.}), \tag{1}$$

where $\theta = \boldsymbol{k}_p \cdot \boldsymbol{x} - \omega_p t$. Here $\boldsymbol{k}_p = (k_p, 0)$, with k_p corresponding to the peak of the initial wave spectrum, and $\omega_p = \sqrt{g k_p}$. The coefficients B, B_2, and B_3 are slowly varying functions of time and space, of first, second and third order in wave steepness, respectively. The mean surface elevation $\bar{\eta}$ is also slowly varying in time and space, and is of higher than second order in wave steepness. The higher-order coefficients can be expressed by B and its derivatives, so that we end up with an evolution equation for the first harmonic coefficient B, from which we can reconstruct the actual surface. This reconstruction can be done to first (first harmonic), second (first and second harmonics) or third order (zeroth through third harmonics) in the wave steepness.

Length and time are scaled by k_p^{-1} and ω_p^{-1}, respectively. Also, $k_p \eta \to \eta$ and $\boldsymbol{k}/k_p \to \boldsymbol{k}$. The initial wave spectrum has the form $F(\boldsymbol{k}) = F(k, \phi) = S(k)D(\phi)$, where k, ϕ are polar coordinates in the $\boldsymbol{k}$-plane. For $S(k)$ we use a JONSWAP spectrum,

$$S(k) = \frac{\alpha}{k^4} \exp\left[-\frac{5}{4}k^{-2}\right] \gamma^{\exp[-(\sqrt{k}-1)^2/(2\sigma_A^2)]}. \tag{2}$$

Here γ is the so-called peak enhancement coefficient and the parameter σ_A has the standard values: 0.07 for $k < 1$ and 0.09 for $k > 1$. The dimensionless parameter α in (2) is chosen such that the steepness, s, has a desired value. In the scaled variables, the steepness s is defined as $\sqrt{2}\sigma$, where

$$\sigma = \left(\int_{\boldsymbol{k}} F(\boldsymbol{k}) \, k \, dk \, d\phi\right)^{1/2} \tag{3}$$

is the scaled standard deviation of the first-order surface.

The angular distribution $D(\phi)$ is taken to be of the form

$$D(\phi) = \begin{cases} \dfrac{1}{\beta} \cos^2\left(\dfrac{\pi\phi}{2\beta}\right), & |\phi| \leqslant \beta, \\ 0, & \text{elsewhere,} \end{cases} \tag{4}$$

where β is a measure of the directional spreading, as illustrated in figure 1.
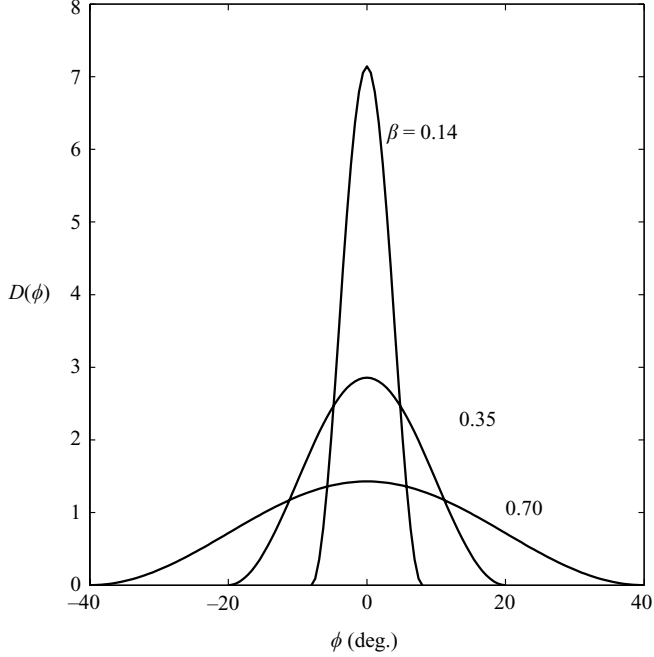
FIGURE 1. The angular distributions (equation (4)) of the initial spectra.

The simulation model uses an origin of the k-plane located at the initial spectral peak and we write $K = k - (0, 1)$. Moreover, the model (see Trulsen *et al.* 2000) employs a cut-off at some $K_c \leqslant 1$ and we have used $K_c = 1$. How much of the energy in the JONSWAP spectrum that is left out depends mainly on γ, and here it is less than 20%.

To solve the modified NLS equation for B we use the numerical method described by Lo & Mei (1985, 1987) with periodic boundary conditions. For all simulations shown in this paper a uniform numerical grid in both horizontal directions with $N_x = N_y = 256$ points, has been used. The discretization of the wavenumber plane is $\Delta K_x = \Delta K_y = 1/128$ where, however, only the modes with $|K| < 1$ are used. The corresponding spatial resolution is hence $\Delta x = 2\pi/(N_x \Delta K_x)$, and similarly for Δy, thus covering 128 characteristic wavelengths in each horizontal direction.

The computations are initiated by specifying the spatial Fourier transform of B, $\widehat{B}$, at $t = 0$,

$$\widehat{B}(\boldsymbol{K}_{mn}, 0) = \sqrt{2F(\boldsymbol{K}_{mn})\Delta K_x \Delta K_y}\, e^{i\theta_{mn}},$$

where the phases θ_{mn} are taken to be uniformly distributed on $[0, 2\pi)$, and $\boldsymbol{K}_{mn} = (K_{xm}, K_{yn}) = (m\Delta K_x, n\Delta K_y)$. The relation between the physical amplitude $B(\boldsymbol{x}_{jk}, t)$ and $\widehat{B}(\boldsymbol{K}_{mn}, t)$ is obtained through the discrete Fourier transform,

$$B(\boldsymbol{x}_{jk}, t) = \sum_{m=-N_x/2, n=-N_y/2}^{N_x/2, N_y/2} \hat{B}(\boldsymbol{K}_{mn}, t) e^{i\boldsymbol{K}_{mn} \cdot \boldsymbol{x}_{jk}}. \tag{5}$$

In order to have a truly Gaussian initial condition, each Fourier coefficient should be chosen as an independent complex Gaussian variable with a variance proportional to the corresponding value of the spectrum. However, numerical experiments using

Case	β	γ
A	0.7	3.3
B	0.35	5
C	0.14	5

TABLE 1. Initial directional and JONSWAP parameters for three simulation cases used to demonstrate the temporal evolution of the spectra. All spectra are normalized to an initial steepness $s = 0.1$.

complex Gaussian Fourier coefficients, unlike using a uniformly distributed phase only, yielded virtually identical time evolutions of the spectrum.

The spectra shown below are obtained as the squared modulus of the Fourier coefficients smoothed with a moving average Gaussian bell with standard deviation $1.7\Delta K_x$. Our computations conserve the total energy and momentum to high accuracy within the bandwidth constraint. We do not, however, account for coupling with free-wave Fourier modes outside the bandwidth constraint. Moreover, the model is based on a perturbation expansion (e.g. Trulsen & Dysthe 1996) that only allows for a limited time horizon, τ, for the calculations of the order of $(\omega_p s^3)^{-1}$, where $\omega_p = 2\pi/T_p$. Quantitative comparisons with wave tank experiments and other numerical wave models (Lo & Mei 1985; Trulsen & Stansberg 2001; Shemer *et al.* 2001, 2002; Stocker & Peregrine 1999; Clamond & Grue 2002) have indicated that a reasonable time horizon is indeed $\tau \approx (\omega_p s^3)^{-1}$, which for the present simulations (with $s = 0.1$) gives $\tau \approx 150 T_p$.

Within these limits, our model appears to be in very good agreement with the physical and numerical experiments mentioned. Due to its very high efficiency it is well-suited for large computational domains and repeated simulations.

3. The temporal evolution of the spectrum

In the simulations presented here we have taken the r.m.s. steepness s to be 0.1, which seems to be a fairly extreme value. This is demonstrated by the (T_p, H_s) scatter diagram in figure 2, where curves of constant steepness are also plotted. It contains approximately 70 000 data points, each representing a 20 min. wave record from the northern North Sea (Pooled data 1973–2001, from the Brent, Statfjord, Gullfaks and Troll platforms).

Three different simulation cases, ranging from a broad to very narrow directional spread, are listed in table 1.

Examples of the temporal evolution for the directional as well as the directionally integrated k-spectra are shown in figures 3–5. As can be seen from the figures, a certain evolution of the spectra takes place over time, with most of the action taking place during the first 70 wave periods. The peak region is broadened along with a small downshift of the peak. For the Gaussian-shaped initial spectrum (Dysthe *et al.* 2003), there was a clear tendency towards a $k^{-2.5}$ power law in the high-wavenumber spectral 'tail'. For the present case such a tendency is still there as can be seen from the figures.

4. The probability distribution of the surface

In the following we investigate the probability distributions of the surface elevation and the crest height. Distributions of simulated data are compared to second-order
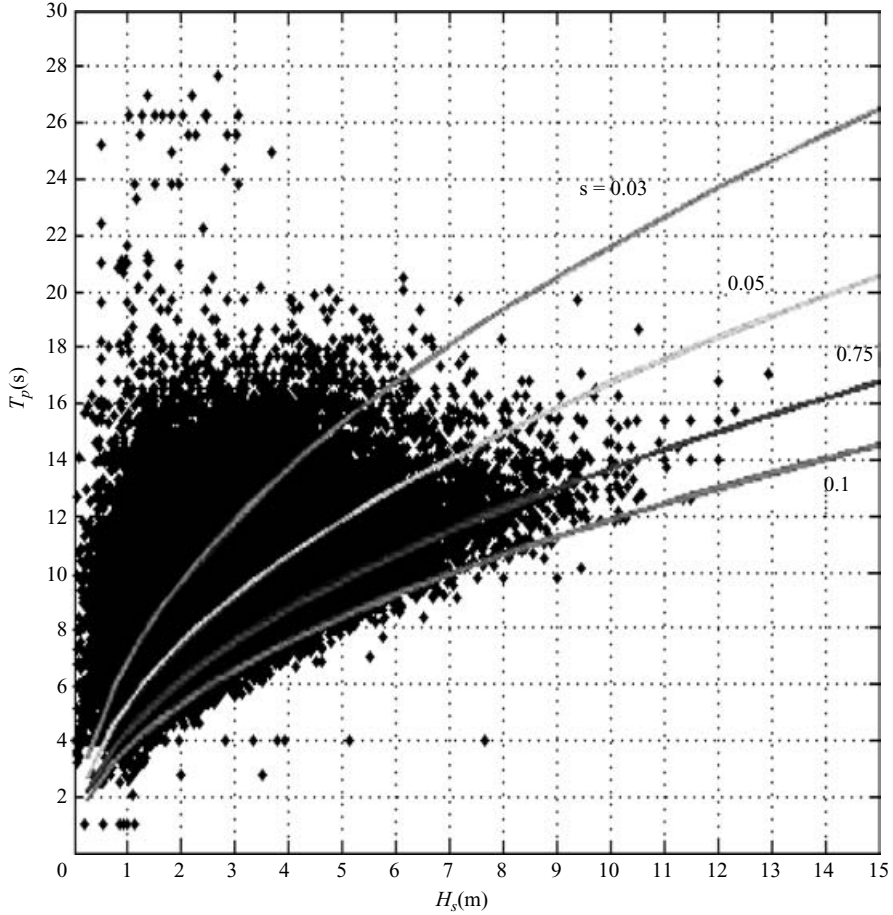
FIGURE 2. Scatter diagram for H_s and T_p from the northern North Sea. Pooled data 1973–2001, from the platforms Brent, Statfjord, Gullfax and Troll. Curves of constant steepness s are also shown. The figure was prepared by K. Johannessen Statoil.

theoretical results due to Tayfun (1980). These results are based on the assumption that the first harmonic in the narrow band development (equation (1)) is Gaussian. This is found to be in very good agreement with the simulations up to 4 standard deviations (4σ) for case A and 3σ for the cases B and C. Virtually no time variation is detected in these ranges of the distributions. In figure 6 the Gaussian probability distribution function (normalized by the standard deviation σ) is compared to typical data of the first harmonic for the cases A, B and C.

4.1. *The distribution of the surface elevation*

In the remainder of the paper it is convenient to scale the surface elevation by the standard deviation σ defined in equation (3). Doing so, and noting that $B_2 = \frac{1}{2}\sigma B^2$, we then have from equation (1) to second order that

$$\eta = \frac{1}{2}(Be^{i\theta} + \frac{\sigma}{2}B^2 e^{2i\theta} + \text{c.c.}) + o(\sigma^2)$$

$$= a\cos(\theta + \psi) + \frac{\sigma}{2}a^2\cos(2\theta + 2\psi) + o(\sigma^2), \qquad (6)$$

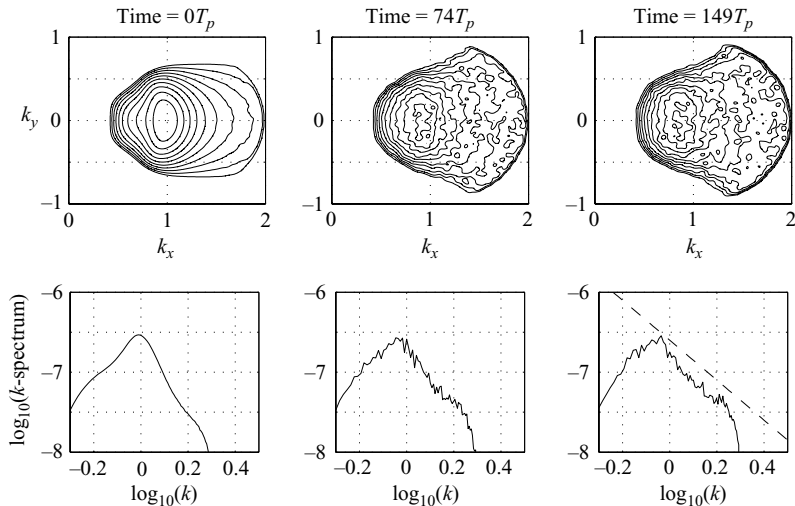where the complex amplitude B of the first harmonic is written $B = a\exp(i\psi)$.

FIGURE 3. The spectral evolution of a truncated JONSWAP spectrum with $\gamma = 3.3$ and $\beta = 0.7$ (case A). The dashed line is the power law $k^{-2.5}$.
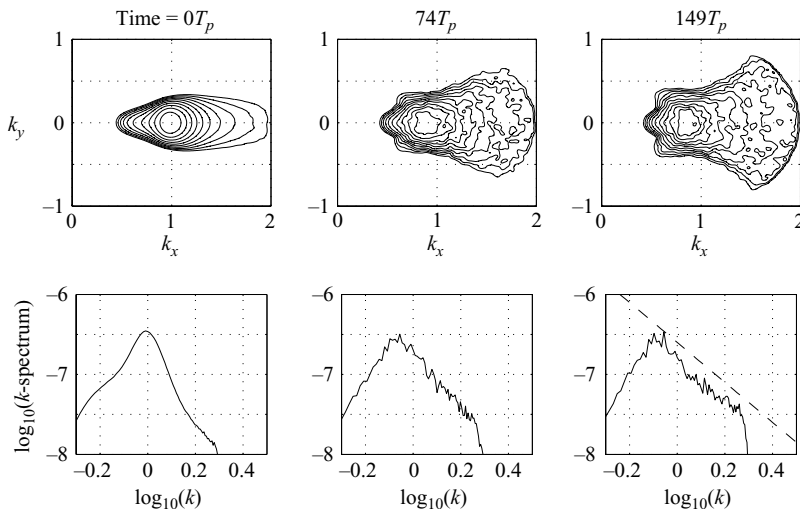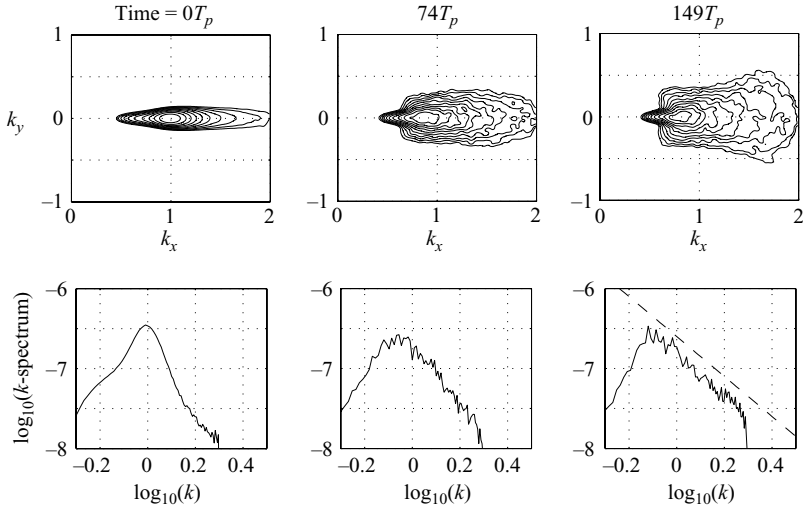

FIGURE 4. Same as figure 3 but with $\gamma = 5$ and $\beta = 0.35$ (case B).

The assumption about normality of the leading-order (linear) approximation was the core of Longuet-Higgins' classical papers from the 1950s. Tayfun (1980) considered a second-order modification of this result while keeping the assumption that the first harmonic B is Gaussian. This implies that the real and imaginary parts $x = a\cos(\theta + \psi)$ and $y = a\sin(\theta + \psi)$ are Gaussian with the joint distribution

$$\frac{1}{2\pi} \exp\left(-\frac{x^2 + y^2}{2}\right).$$

Since to second order,

$$\eta = a\cos(\theta + \psi) + \frac{\sigma}{2}a^2(\cos^2(\theta + \psi) - \sin^2(\theta + \psi)),$$

FIGURE 5. Same as figure 3 but with $\gamma = 5$ and $\beta = 0.14$ (case C).
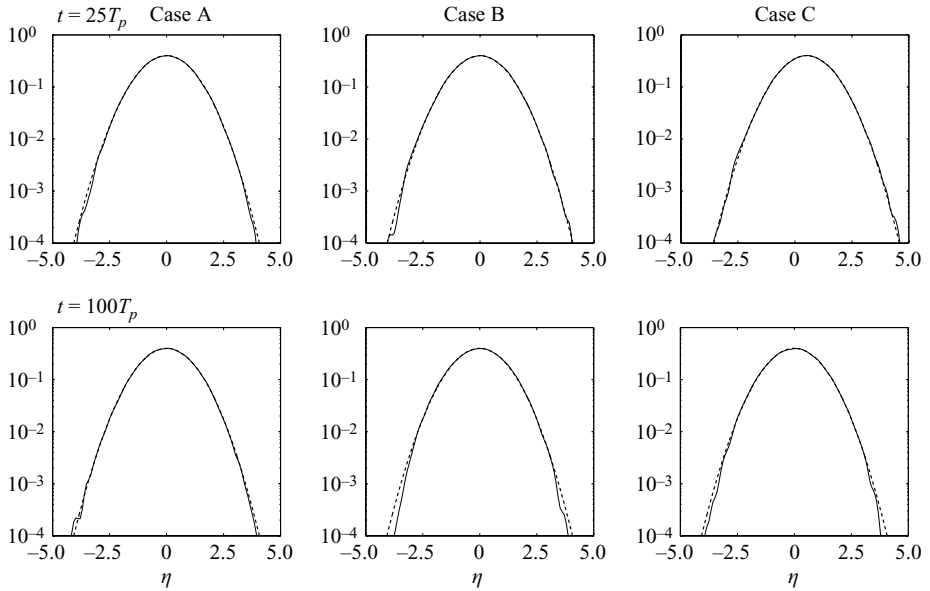
FIGURE 6. Typical simulated distributions of the first harmonic for cases A, B and C (scaled with σ) at two different times, compared to a Gaussian distribution.

the cumulative distribution $P(z)$ of η is given by

$$P(z) = \frac{1}{2\pi} \int_{x + \frac{\sigma}{2}(x^2 - y^2) \leqslant z} \exp\left(-\frac{x^2 + y^2}{2}\right) \mathrm{d}x \, \mathrm{d}y.$$
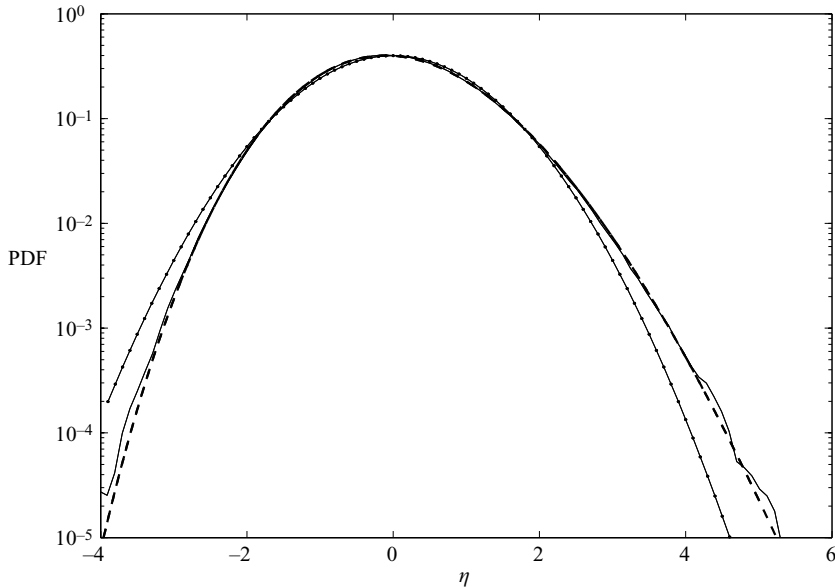
FIGURE 7. Typical simulated distribution (solid line) of the surface elevation for case A (scaled with σ) compared to the Gaussian distribution equation (8) (solid with dots) and the Tayfun (dashed) distribution defined in equation (7). $t = 75T_p$.

After some calculation, one obtains the probability distribution $p_\eta = \mathrm{d}P/\mathrm{d}z$ as

$$
\begin{aligned}
p_\eta(z) &= \frac{1}{\pi\sigma} \int_0^\infty \left(\exp\left[-\frac{x^2 + (1-C)^2}{2\sigma^2} \right] + \exp\left[-\frac{x^2 + (1+C)^2}{2\sigma^2} \right] \right) \frac{\mathrm{d}x}{C} \\
&\simeq \frac{1}{\pi\sigma} \int_0^\infty \exp\left[-\frac{x^2 + (1-C)^2}{2\sigma^2} \right] \frac{\mathrm{d}x}{C},
\end{aligned}
\tag{7}
$$

where

$$
C = \sqrt{1 + 2\sigma z + x^2}.
$$

The same result (given in a more awkward form) was also found by Tayfun (1980).

Using the fact that $\sigma^2 \ll 1$, the integral in equation (7) can be expanded asymptotically. By the Laplace method the leading term is found to be

$$
p_\eta(z) \sim \frac{1 - 7\sigma^2/8}{\sqrt{2\pi(1 + 3G + 2G^2)}} \exp\left(-\frac{G^2}{2\sigma^2} \right),
\tag{8}
$$

where

$$
G = \sqrt{1 + 2\sigma z} - 1.
$$

Numerically, it has been found to be a very good approximation to (7). Note that the asymptotic form (8) has the mild restriction $\eta > -3/(8\sigma)$.

Figure 7 shows a comparison of (8) with typical data from simulation A. It is seen that the correspondence is remarkable at least up to 4 standard deviations. For cases B and C the agreement was good up to 3 standard deviations. The simulated data used in the figure are from one 'snapshot' (in time) of our 'artificial ocean', covering roughly 10.000 waves. Taking such 'snapshots' (henceforth referred to as a 'scene') at various instances of time during the evolution process of the wave spectrum, practically no

variations could be seen for case A when $\eta < 4$ and for the cases B and C when $\eta < 3$. Note that in cases B and C the number of waves in one scene are reduced.

Srokosz & Longuet-Higgins (1986) also used the assumption of a Gaussian-distributed first harmonic to calculate the skewness $\overline{\eta^3}$ to second order in the wave steepness. Their result for the narrow-band case (also using the scaling $\eta \to \eta/\sigma$) is

$$\overline{\eta^3} = 3\sigma. \tag{9}$$

The result follows readily by averaging η^3, with η given by the first two terms in equation (6), and assuming that the first harmonic is Gaussian.

An expression for the kurtosis $\overline{\eta^4}$ can be derived in the same way giving

$$\overline{\eta^4} = 3 + 12\sigma^2. \tag{10}$$

However, expression (10) is not consistent, since third-order terms will also give contributions of $O(\sigma^2)$. If only the third-order Stokes contribution is taken into account the coefficient would be 24 instead of 12. In our simulations with $\sigma = 0.071$ we find the skewness to be in the range 0.19 to 0.21. The corresponding value obtained from (9) is 0.213.

For a narrow angular distribution $\beta = 0.14$ ($\pm 4°$), the kurtosis shows a co-variation with the abundance of large waves (see figures 11–13 below). For a relatively broad angular distribution $\beta = 0.7$ ($\pm 20°$), we find the variation to be very small, in the range 3.04 to 3.11. The value obtained from (10) is 3.06.

4.2. *The distribution of the wave crests*

In the narrow-band numerical model we are computing the development of the first-harmonic complex amplitude, B. From knowledge of B the wave field and its upper and lower envelopes can be constructed up to third order in wave steepness. Since the equations are invariant with respect to transformation $B \to B \exp(i\xi)$, where ξ is a real constant, the construction of the wave field contains an arbitrary constant phase shift. By varying the phase shift between 0 and 2π, the curves of contact between the envelopes and the wave field generate the envelope surfaces. For the narrow-band case the curves of contact on the upper envelope are very close to the 'crests' of the wave field. This means that, at a given time, any point on the upper envelope is on the crest of a possible wave field. Thus, we shall take the distribution of wave crests to mean the distribution of the upper envelope. Other definitions are possible, e.g. to associate the crest height with the highest point on a 'wave-ridge'.

Up to second order in wave steepness, and with a scaling in terms of σ as discussed above, the second-order upper surface envelope is given by

$$A \equiv a + \frac{\sigma}{2}a^2, \tag{11}$$

where $a \equiv |B|$. Following Tayfun (1980), B is again assumed to be complex Gaussian so that a is Rayleigh distributed,

$$p_a(a) = a \exp\left(-\frac{a^2}{2}\right). \tag{12}$$

Because of the relation between a and A in (11), their respective distributions p_a and p_A satisfy the relation
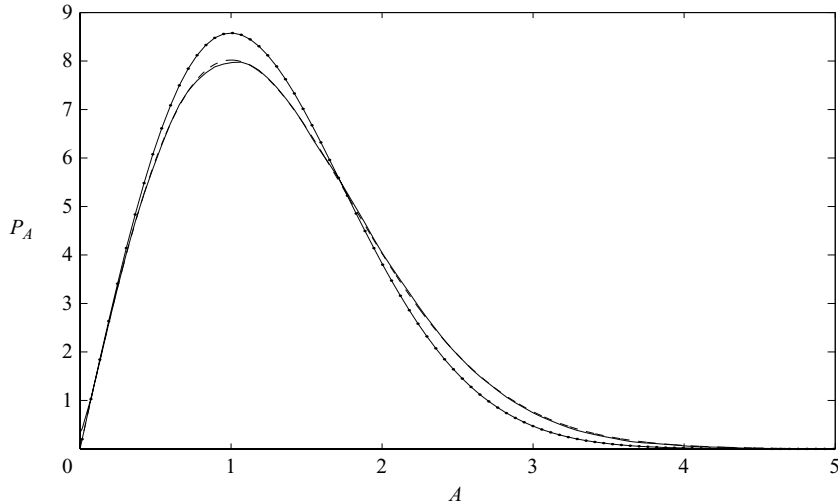
$$p_A \, \mathrm{d}A = p_a \, \mathrm{d}a. \tag{13}$$

FIGURE 8. Typical simulated distribution of the crest height (scaled with σ) for case A (solid), compared to the distributions of Tayfun equation (14) (dashed) and Rayleigh (solid with dots). $t = 100T_p$.

Thus,

$$p_A(A) = \frac{1}{\sigma}\left(1 - \frac{1}{\sqrt{2\sigma A + 1}}\right)\exp\left[-\frac{1}{\sigma^2}(\sigma A + 1 - \sqrt{2\sigma A + 1})\right]. \qquad (14)$$

Distribution (14) was found by Tayfun (1980) and has been called a Rayleigh–Stokes distribution (Nerzic & Prevosto 2000). Here we shall refer to (8) and (14) as the Tayfun distributions of surface elevation and crest height, respectively. It is readily verified that in the limit $\sigma \to 0$, expression (8) tends to the Gaussian distribution $\exp(-z^2/2)/\sqrt{2\pi}$, and expression (14) tends to the Rayleigh distribution $A\exp(-A^2/2)$. For comparisons of (14) with data from storm waves, see Warren, Bole & Drives (1998).

In figure 8 the Tayfun distribution, p_A, is compared to typical results from simulations of case A. Also the Rayleigh distribution is shown for comparison. It is seen that p_A fits the data very well for the bulk of the distribution ($A < 4$, say). Similar to the distribution of the surface elevation η, that of the crest height A, constructed from 'snapshots' of the simulation domain taken at various times, shows practically no variations for $A < 4$. For cases B and C the approximate time invariance is limited to $A < 3$.

While the bulk of the distribution seems to be virtually time independent during the spectral development, this is not obvious for the extremes parts. In figure 9 we show the observed probability of exceedance for the crest height, A (scaled with σ). This is compared with the Rayleigh and Tayfun probabilities of exceedance given by

$$P_R(A > x) = \exp(-x^2/2), \qquad (15)$$

$$P_T(A > x) = \exp\left[-\frac{1}{\sigma^2}(\sigma x + 1 - \sqrt{2\sigma x + 1})\right], \qquad (16)$$

respectively. A large deviation from the Tayfun distribution is seen only in case C for $A > 3$. This happens in the first phase of the spectral change. Note that for the long-crested case, C, the number of waves in each scene is reduced.
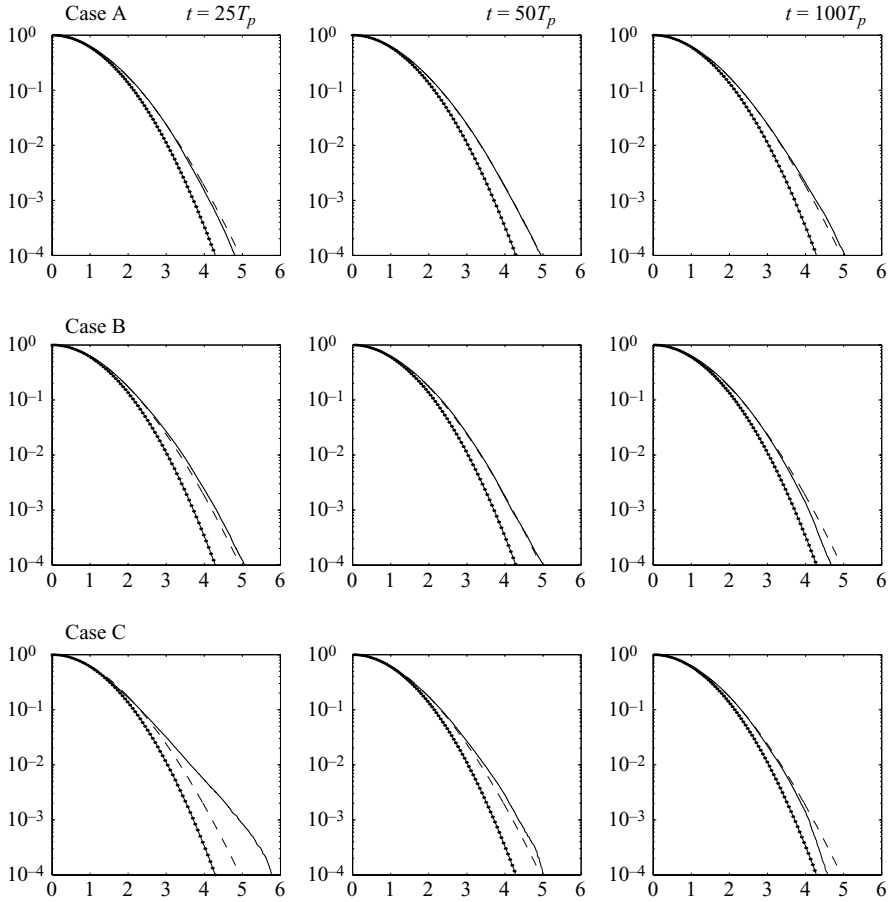
FIGURE 9. Simulated probability of exceedance of the scaled crest height (solid) compared to the Rayleigh (solid with dots) and Tayfun (dashed) probabilities defined in equations (15) and (16). For cases A–C at these different times.

4.3. *The distribution of extremes*

For up to four times the standard deviation of the surface, we have shown that the simulated data fit the Tayfun distributions very well both for the surface elevation (8) and the crest height (14). This does not seem to change with time despite the fact that the spectrum is changing.

In the following, we compare the data of the very extreme waves with the corresponding theoretical predictions. Our starting point is a theorem due to Piterbarg (1996) which states the asymptotic extremal distributions for homogeneous Gaussian fields in n free variables. Below we shall only consider the two-dimensional case ($n = 2$), where the stochastic variable is the sea surface elevation η. Let S be an area of the ocean corresponding to a part of the computational domain. The surface elevation (at any given instant of time) attains its maximum η_m at some point in S. The theorem gives the distribution of η_m over independent realizations of the surface, assuming the surface elevation to be Gaussian. Obviously, the distribution of η_m depends on the size of S. This size is conveniently measured in terms of the 'number of waves', N, that it contains. The size of one 'wave' is $\lambda_0 \lambda_c / \sqrt{2\pi}$, where λ_0 is the

mean wavelength and λ_c the mean crest length defined in terms of the wave spectrum $F(k_x, k_y)$ as

$$\lambda_0 = \frac{2\pi}{\langle k_x^2 \rangle^{1/2}}, \quad \lambda_c = \frac{2\pi}{\langle k_y^2 \rangle^{1/2}},$$

where

$$\langle k_{x,y}^2 \rangle = \frac{\int k_{x,y}^2 F(k_x, k_y) \, \mathrm{d}k_x \, \mathrm{d}k_y}{\int F(k_x, k_y) \, \mathrm{d}k_x \, \mathrm{d}k_y}.$$

The size of the computational domain, S, is $N_x N_y \lambda_p^2$. Thus, the number of 'waves' is

$$N = \sqrt{2\pi} \frac{N_x N_y \lambda_p^2}{\lambda_0 \lambda_c} = \sqrt{2\pi} N_x N_y \frac{(\langle k_x^2 \rangle \langle k_y^2 \rangle)^{1/2}}{k_p^2}.$$

In the present simulations $N_x = N_y = 128$, giving $N \sim 10^4$ for the full domain (varying somewhat with the angular distribution of the spectrum).

Piterbarg's theorem states that the asymptotic cumulative distribution of η_m for realizations of such a Gaussian ocean containing N waves is

$$P(\eta_m \leqslant x, N) \sim \exp\left[-\frac{x}{h_N} \exp\left(-\tfrac{1}{2}(x^2 - h_N^2)\right)\right], \tag{17}$$

where h_N is a solution of the equation $h \exp(-h^2/2) = 1/N$, that is,

$$h_N = \sqrt{2 \ln N + \ln(2 \ln N + \ln(2 \ln N + \cdots))}.$$

From computer simulations of Gaussian surfaces with ocean-wave-like spectra, (17) has been found to be very accurate indeed (see e.g. Krogstad *et al.* 2004).

We have previously observed that the complex amplitude, B, of the first harmonic is Gaussian to a good approximation for $|B| < 4\sigma$. The maximum of the second-order surface elevation η_m is obviously found at a wave crest. Thus, denoting the elevation of the first-order reconstructed surface by η_1, the relation between the first- and second-order maxima, η_{1m} and η_m is, according to (11), given by $\eta_m = \eta_{1m} + \tfrac{1}{2}\sigma \eta_{1m}^2$, or $\eta_{1m} = (1/\sigma)(\sqrt{1 + 2\sigma \eta_m} - 1)$. The asymptotic distribution of the second-order surface is then obtained from (17) after applying the transformation

$$x \to \frac{1}{\sigma}(\sqrt{1 + 2\sigma x} - 1). \tag{18}$$

We shall refer to this as the Piterbarg–Tayfun distribution.

In figure 10 we compare the predicted values from this modified Piterbarg distribution with the simulations for case A.

The asymptotic Gumbel limit of the Piterbarg–Tayfun distribution is easily found to be

$$\exp\left[-\exp\left(-\frac{h_N - 1/h_N}{1 + \sigma h_N}\left(x - \left(h_N + \tfrac{1}{2}\sigma h_N^2\right)\right)\right)\right],$$

and the corresponding expected value of η_m is then

$$E(\eta_m) \simeq h_N + \frac{\sigma}{2} h_N^2 + \frac{\gamma(1 + \sigma h_N)}{h_N - 1/h_N}, \tag{19}$$
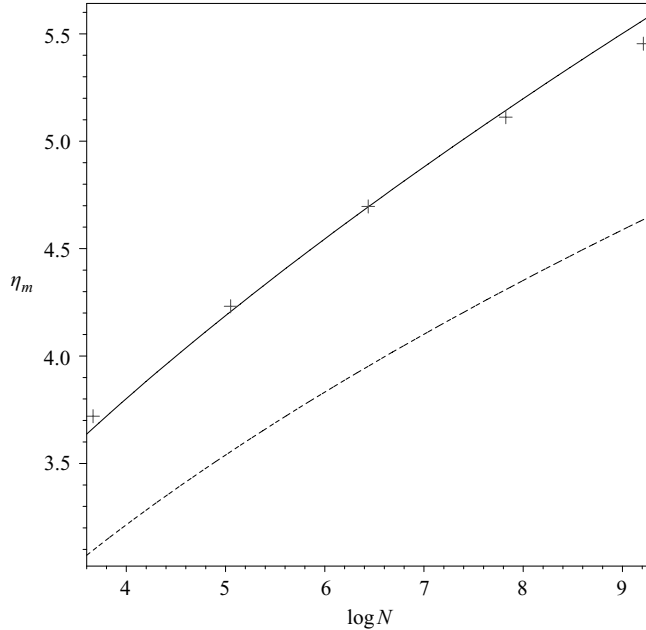
FIGURE 10. The average largest surface elevation of scenes containing N waves. Simulations, case A, (crosses) are compared with the expected value given by equation (19) for $\sigma = 0.071$ used in the simulations (solid), and $\sigma = 0$ corresponding to the Gaussian case (dashed).

where $\gamma \simeq 0.5772$ is the Euler–Macheroni constant. Each point in the figure is the average value of η_m from roughly 100 simulation scenes of the same size. The sizes of the scenes in terms of the 'number of waves' ranges from 40 to 10 000. (As a comparison, a 20 min. wave record of storm waves (T_p in the range 8–12 s) contains 100–150 waves.)

As can be seen from the figure, there is good agreement with the Piterbarg–Tayfun distribution up to five standard deviations.

4.4. *Influence of spectral change*

Spectral change due to the modulational- or Benjamin-Feir-type instability has been linked by theory and simulations with the enhanced occurrence of large waves (Onorato *et al.* 2000; Mori & Yasuda 2000; Janssen 2003).

Recently, Onorato *et al.* (2004) have performed experiments in a long wave flume with a JONSWAP-type spectrum being generated at one end. They consider cases with different ratios between the r.m.s. steepness s and the relative spectral bandwidth Δ_ω. Following Janssen (2003) they call this ratio the Benjamin–Feir index (BFI) (i.e. $BFI \equiv s/\Delta_\omega$).† For $BFI \gtrsim 1$ they see an increase in the number of large waves at fetches where the spectrum is changing. There is also a co-variation between the occurrence of large waves and the kurtosis.

In the simulations we find good qualitative agreement with the experiment of Onorato *et al.* (2004) when the initial angular distribution is very narrow ($\beta = 0.14$, ($\pm 4°$)). This is demonstrated for three runs in figures 11–13. The first one has $\gamma = 3.3$ and $BFI = 1.03$, whereas the two others with $\gamma = 5$ ($BFI = 1.24$) differ only by the

---

† Their definition of the relative spectral bandwidth is $\Delta_\omega = \Delta\omega/\omega_p$ where $\Delta\omega$ is the half-width at half the peak value of the spectrum. This is slightly different from Janssen's definition.
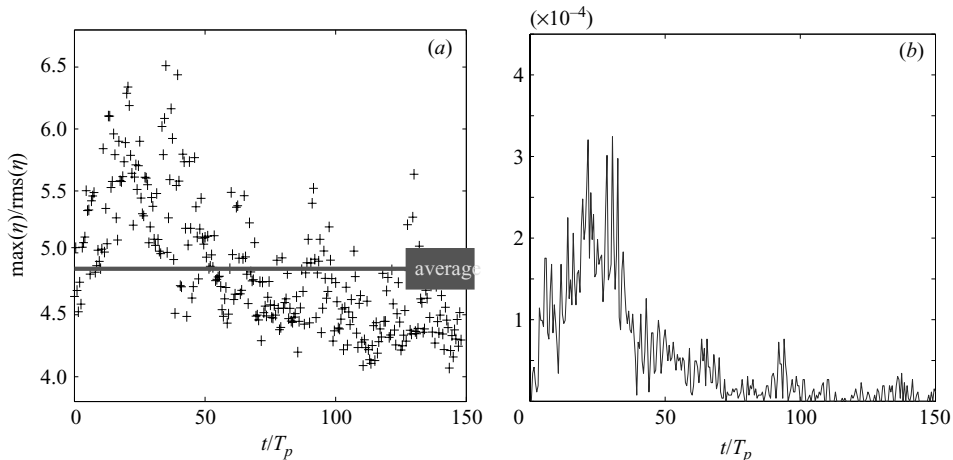
FIGURE 11. (*a*) Maximum elevation η_m for the full scene ($\sim 10^4$ waves) taken every half a wave period ($T_p/2$). (*b*) The relative number of data points above 4.4 standard deviations ('freaks'). Here $\gamma = 3.3$, $\beta = 0.14$ and $BFI = 1.03$.
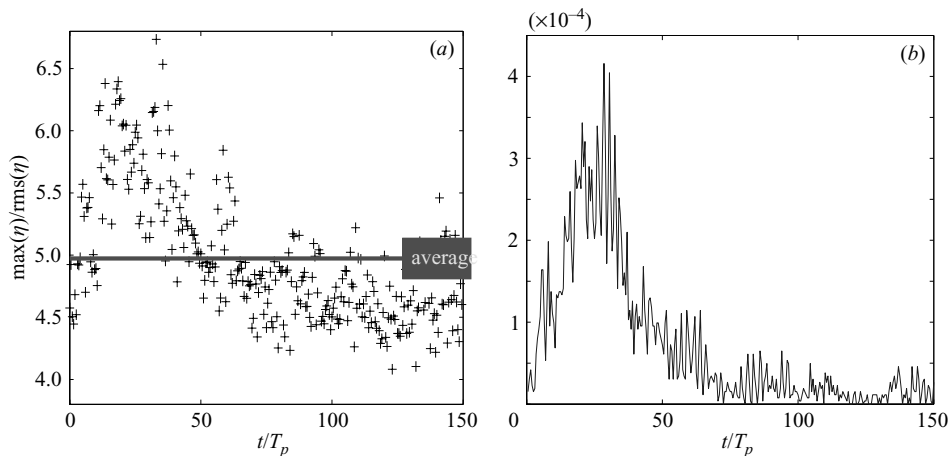

FIGURE 12. Same as figure 11 but with $\gamma = 5$, $\beta = 0.14$, and $BFI = 1.24$.

random choice of initial phases. Figures (11*a*)–(13*a*) show the maximum elevation η_m for our computational domain at time intervals of $T_p/2$ for the three runs. For the same runs, figures (11*b*)–(13*b*) show the relative number of data points with $\eta > 4.4\sigma$ ('freaks' according to the criteria in equation (20)). It is seen that the occurrence of large waves is significantly increased while the main spectral change is taking place (the first $50T_p$). A similar variation in the kurtosis can be seen in figure 14.

For short-crested waves, however, the influence of spectral change seems rather insignificant even if $BFI > 1$. This is demonstrated in figures 15–17. The three runs with $\beta = 0.7$ ($\pm 20°$) and $\gamma = 3.3$. ($BFI = 1.03$) differ only by the initial random choice of phases. In contrast to the above results for long-crested waves, there does not seem to be any clear trend. The same is true for the kurtosis as shown in figure 18. Here we have included curves for cases B and C for comparison.
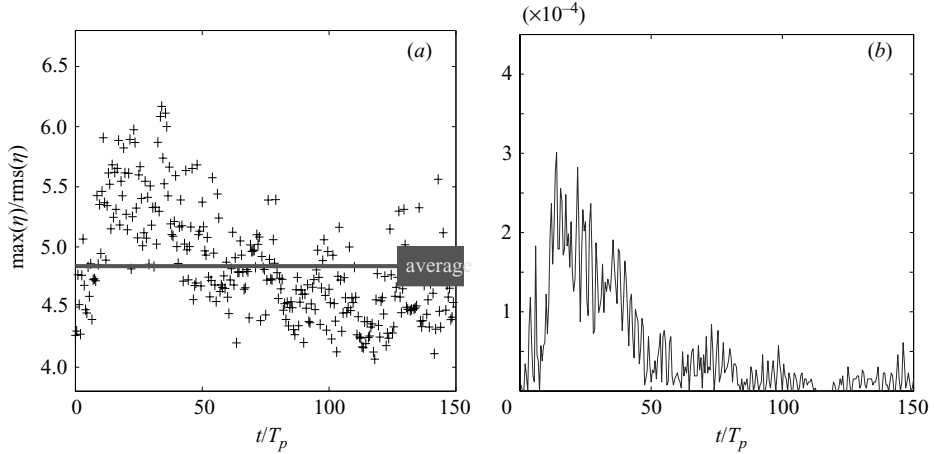
FIGURE 13. Same as figure 12 but with different initial phases.
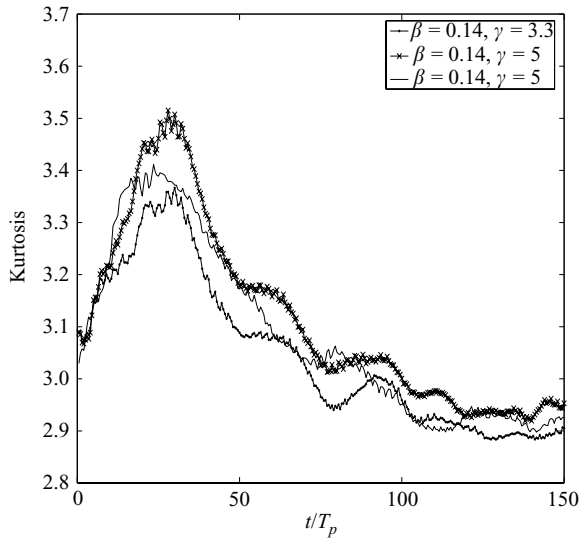

FIGURE 14. The kurtosis for the cases in figures 11–13.

It was shown by Onorato, Osborne & Serio (2002) by small-scale simulations using the higher-order NLS equation that with increase of the angular spread, the occurrence of extreme events decreased. To some extent this tendency is confirmed by our simulation, which can be seen by comparing figures 11–13 to the corresponding figures 15–17 (note the change of scales).

4.5. *The extreme group*

Both empirical data and simulations indicate that the wave group in which an extreme wave occurs is rather short, containing on the average only one big wave. In a sense this group is a more important object than the large wave it contains because it has a longer lifetime than the individual large wave. Roughly one period T_p after the realization of an extreme crest height, the characteristic feature of the same group
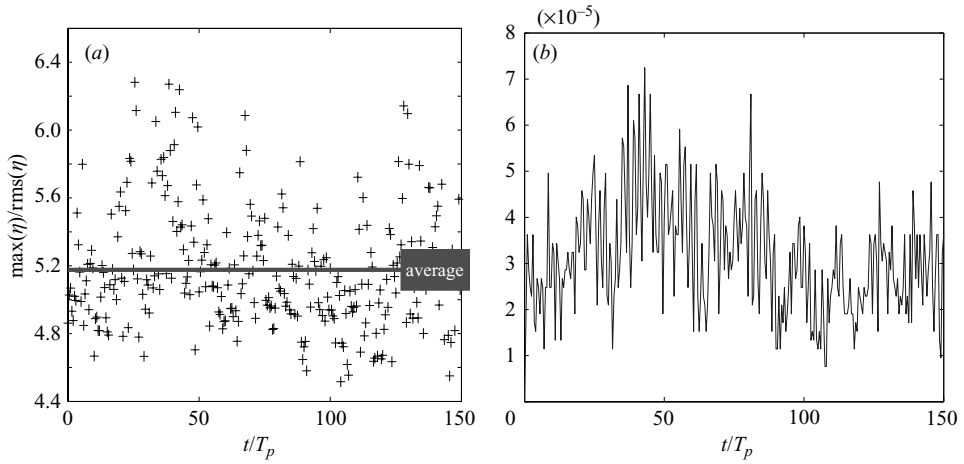
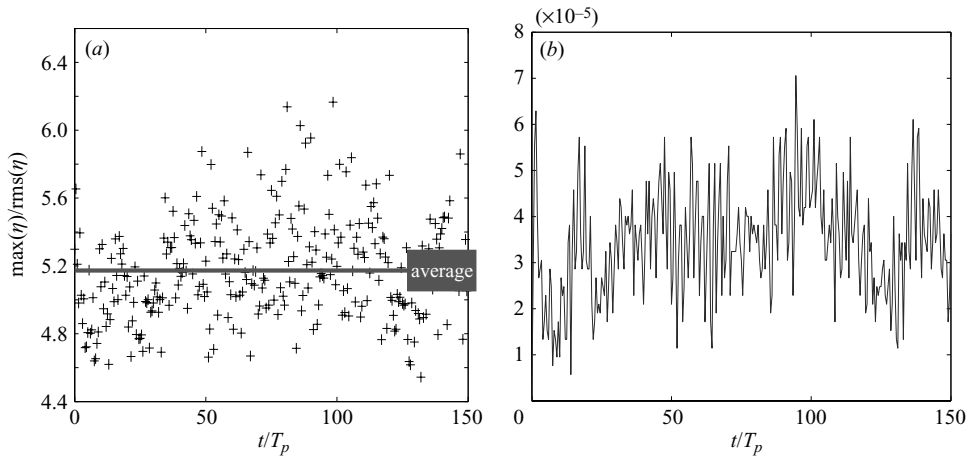FIGURE 15. As figure 11 but with $\gamma = 3.3$ and $\beta = 0.7$, and $BFI = 1.03$.

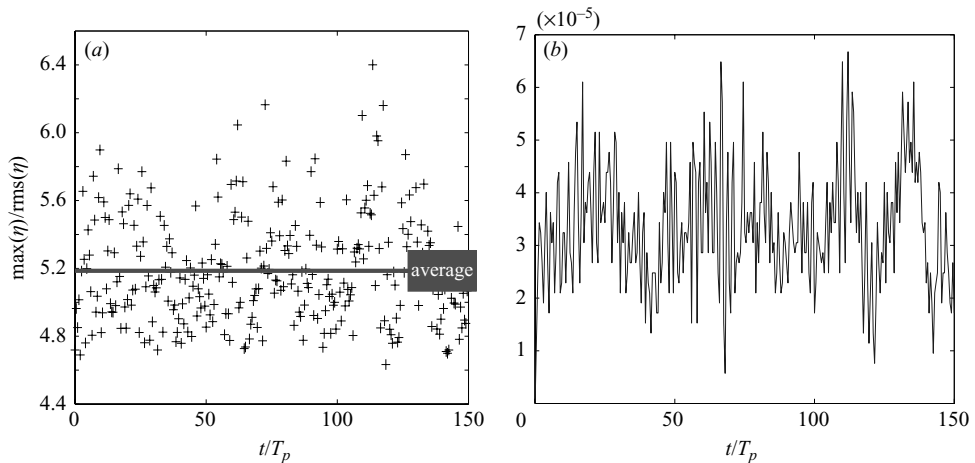FIGURE 16. Same as figure 15 but with different initial phases.

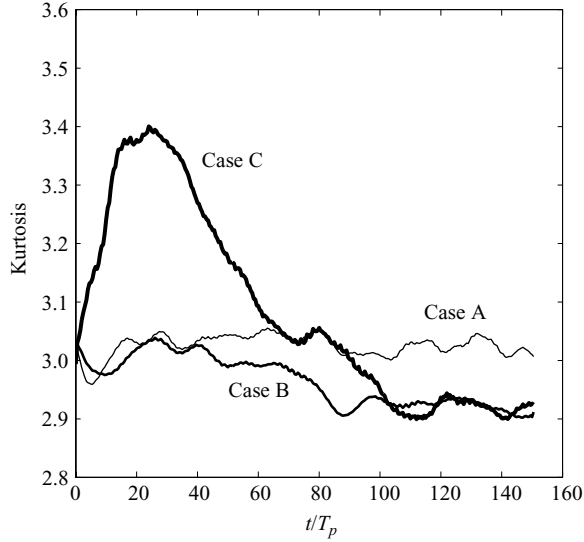FIGURE 17. Same as figure 15 but with different initial phases.

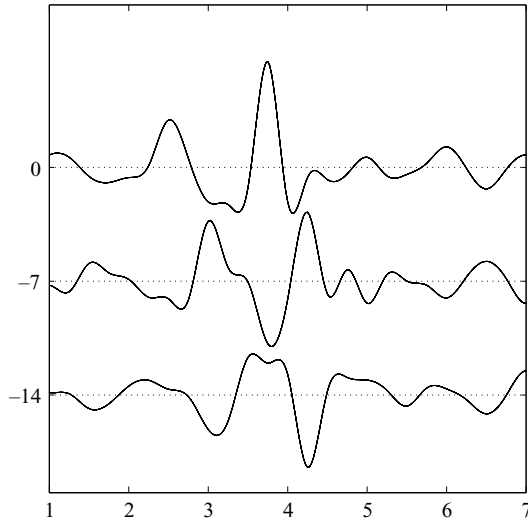FIGURE 18. Development of the kurtosis for the three cases A, B and C.

FIGURE 19. Snapshots of an extreme wave event taken at intervals $T_p/2$ with cuts along the main wave propagation direction.

will be a deep trough (a 'hole in the ocean'). An example is illustrated in figure 19, where three snapshots at intervals $T_p/2$ are shown.

In the following we consider effects related to groups containing extreme waves, starting with some empirical results by Skourup, Andreasen & Hansen (1996). They analysed more than 1600 hours of storm wave records from the central North Sea (the Gorm field). The waves satisfying one of the following two criteria:

$$A > 1.1H_s \quad \text{or} \quad H > 2H_s \tag{20}$$

were denoted 'freaks', where H is the wave height and $H_s = 4\sigma$ is the significant wave height. The number of waves found to satisfy the first criterion was 446 while only
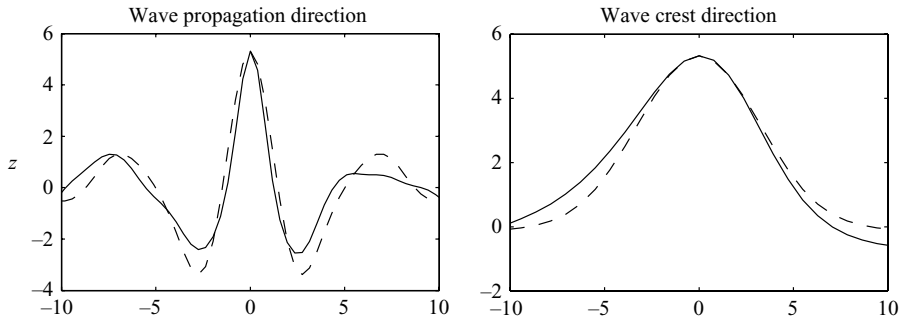
FIGURE 20. Cuts through the maximum of the average wave profile in the main wave and crest directions (full curves), compared with the the spatial covariance function (dashed curve). Simulation A.

51 satisfied the second one. The ratio $446/51 \simeq 8.7$ is then a rough estimate of the probability ratio between the two events in equation (20). To make a comparison we assume that the distribution of H

$$P(h > H) = \exp(-H^2/\overline{H^2}). \tag{21}$$

For an extremely narrow spectrum, $\overline{H^2} = 4\overline{a^2} = 8m_0$. When compared to real data, this is known to give too high estimates. Longuet–Higgins (1980), however, fitted the distribution (21) to observational data compiled by Forristall (1978) from storms in the Gulf of Mexico, and demonstrated a good agreement if the variance was chosen as $\overline{H^2} \simeq 6.85m_0$. Later, Næss (1985) generalized this result, relating the correction factor to the first minimum of the correlation function.

Now, using (21) for H (with $\overline{H^2} \simeq 6.85m_0$) and the two distributions (16) for A, we obtain for the Rayleigh distribution $P_R(A > 1.1H_s)/P(H > 2H_s) \simeq 1.4$, while for the Tayfun distribution with $\sigma = 0.071$ (corresponding to $s = 0.1$), the ratio is $P_T(A > 1.1H_s)/P(H > 2H_s) \simeq 6.5$. Since the depth at the Gorm field is only around 40 m, the nonlinear effects there may be even stronger than in deep water.

For a Gaussian surface, the average waveform in the neighbourhood of an extreme wave maximum is given by the scaled auto-covariance function, see, e.g. Lindgren (1972). In figure 20, cuts through averaged wave shapes over the maximum in the wave and crest directions are compared to the auto-covariance function. This indicates, in accordance with the above, that on the average, the extreme wave belongs to a very short group, with room only for one big wave. Also, two other differences are obvious: the simulated large crest is more narrow and the troughs next to it are more shallow than indicated by the covariance function. For their collection of 'freaks' Skourup *et al.* found that the average ratio A/H was approximately 0.7. For the cases shown in figure 20 the covariance function prediction is $\simeq 0.6$ and the simulations give $\simeq 0.7$.

5. Conclusions

The three-dimensional simulations reported here have used higher-order NLS-type equations (Dysthe 1979; Trulsen & Dysthe 1996; Trulsen *et al.* 2000), with a computational domain of dimensions 128×128 typical wavelengths, containing about 10^4 waves in the short crested case.

We start with a truncated JONSWAP spectrum with various angular distributions giving both long- and short-crested waves. The Fourier modes (approximately 6×10^4)

are interacting to redistribute the spectral energy. Quite similar results to those reported earlier for bell-shaped initial spectra (Dysthe *et al.* 2003) are found. We see a 'relaxation' of the initial spectrum to a new shape on the Benjamin–Feir timescale $(s^2\omega_p)^{-1}$. The spectral change is more pronounced when the initial spectrum is very narrow (both in terms of the peak enhancement parameter γ and the angular width parameter β).

The probability distributions of crest height and surface elevation are investigated next. For the more realistic short-crested case the distributions from simulated data of elevations and crest heights less than 4 standard deviations (i.e. the significant waveheight H_s) are very represented well by the theoretical second-order distributions proposed by Tayfun (1980). This part of the distributions seems to be virtually time independent even during a phase of spectral change.

For larger waves (elevation higher than H_s) this is not always so. For long-crested waves with relative spectral width Δ_ω less than or near the steepness s, we see an increased density of large waves during spectral evolution.

For short-crested waves, however, the spectral change does not seem to have much influence on the distribution of the large waves. For this case extreme wave analysis indicates that the Tayfun distributions is a good approximation even up to five standard deviations.

REFERENCES

ALBER, I. E. 1978 The effects of randomness on the stability of two-dimensional surface wavetrains. *Proc. R. Soc. Lond.* A **363**, 525–546.

ALBER, I. E. & SAFFMAN, P. G. 1978 Stability of random nonlinear deep water waves with finite bandwidth spectrum. *TWR Defense and Spacesystems Group Rep.* 31326–6035–RU–00.

BENJAMIN, T. B. & FEIR, J. E. 1967 The disintegration of wave trains on deep water. Part 1. Theory. *J. Fluid Mech.* **27**, 417–430.

CLAMOND, D. & GRUE, J. 2002 Interaction between envelope solitons as a model for freak wave formations. Part I: Long time interaction. *C. R. Mec.* **330**, 575–580.

CRAWFORD, D. R., SAFFMAN, P. G. & YUEN, H. C. 1980 Evolution of a random inhomogeneous field of nonlinear deep-water gravity waves. *Wave Motion* **2**, 1–16.

DYSTHE, K. B. 1979 Note on a modification to the nonlinear Schrödinger equation for application to deep water waves. *Proc. R. Soc. Lond.* A **369**, 105–114.

DYSTHE, K. B., TRULSEN, K., KROGSTAD, H. E. & SOCQUET-JUGLARD, H. 2003 Evolution of a narrow-band spectrum of random surface gravity waves. *J. Fluid Mech.* **478**, 1–10.

FORRISTALL, G. A. 1978 On the statistical distribution of wave heights in a storm. *J. Geophys. Res.* **83**, 2553–2558.

HASSELMANN, K. 1962 On the nonlinear energy transfer in a gravity-wave spectrum. Part 1. General theory. *J. Fluid Mech.* **12**, 481–500.

HAVER, S. & ANDERSEN, O. J. 2000 Freak waves, rare realizations of a typical population or a typical realization of a rare population. *Proc. ISOPE Conf.*, 2000 *Seattle.*	Q2

JANSSEN, P. A. E. M. 2003 Nonlinear four wave interaction and freak waves. *J. Phys. Oceanogr.* **33**, 863–884.

KHARIF, C. & PELINOVSKY, E. 2004 Physical mechanisms of the rogue wave phenomenon. *Eur. J. Mech.* B/*Fluids* **22**, 603–634.

KROGSTAD, H. E., LIU, J., SOCQUET-JUGLARD, H., DYSTHE, K. B. & TRULSEN, K. 2004 Spatial extreme value analysis of nonlinear simulations of random surface waves. *Proc. OMAE 2004 Conf.*	Q2

LIGHTHILL, M. J. 1965 Contribution to the theory of waves in nonlinear dispersive systems. *J. Inst. Maths Applics*, **1**, 269–306.

LIGHTHILL, M. J. 1967 Some special cases treated by the Whitham theory. *Proc. R. Soc. Lond*. A **299**, 28–53.

LINDGREN, G. 1972 Local maxima of Gaussian fields. *Arkiv för Matematik* **10**, 195–218.

LO, E. & MEI, C. C. 1985 A numerical study of water-wave modulation based on a higher-order nonlinear Schrödinger equation. *J. Fluid Mech.* **150**, 395–416.

LO, E. Y. & MEI, C. C. 1987 Slow evolution of nonlinear deep water waves in two horizontal directions: A numerical study. *Wave Motion* **9**, 245–259.

LONGUET-HIGGINS, M. S. 1980 On the distribution of the height of sea waves: Some effects of Nonlinearity and finite band width. *J. Geophys. Res.* **85**, 1519–1523.

MORI, N. & YASUDA, T. 2000 Effects of high-order nonlinear wave-wave interactions on gravity waves. *Proc. Workshop on Rogue Waves 2000* (ed. M. Olagnon & G. Athanassoulis) pp. 229–244. IFREMER.

NAESS, A. 1985 The joint crossing frequency of stochastic processes and its application to wave theory. *Appli. Ocean Res.* **7**, 35.

NERZIC, R. & PREVOSTO, M. 2000 A Weibull–Stokes model for the distribution of maximum wave and crest heights. *Proc. 7th ISOPE Conf.* vol. 3, pp. 367–377.

OLAGNON, M. & ATHANASOULIS, G. 2000 (Eds.) *Proc. Workshop on Rogue Waves, 2000*, IFREMER.

ONORATO, M., OSBORNE, A. R. & SERIO, M. 2002 Extreme wave events in directional, random oceanic sea states. *Phys. Fluids* **14**, L25–L28.

ONORATO, M., OSBORNE, A. R., SERIO, M., CAVALERI, L., BRANDINI, C. & STANSBERG, C. T. 2004 Extreme waves and modulational instability: wave flume experiments on irregular waves. *J. Fluid Mech.* (Submitted).

ONORATO, M., OSBORNE, A. R., SERIO, M. & DAMIANI, T. 2000 Occurrence of freak waves from envelope equations in random ocean wave simulations. *Proc. Workshop on Rogue Waves 2000* (ed. M. Olagnon & G. Athanassoulis), 181–191. IFREMER.

PITERBARG, V. I. 1996 Asymptotic methods in the theory of Gaussian processes and fields, *AMS Transl. Math. Monographs.* **148**.

SHEMER, L., JIAO, H. Y., KIT, E. & AGNON, Y. 2001 Evolution of a nonlinear wave field along a tank: experiments and numerical simulations based on the spatial Zakharov equation. *J. Fluid Mech.* **427**, 107–129.

SHEMER, L., KIT, E. & JIAO, H. Y. 2002 An experimental and numerical study of the spatial evolution of unidirectional nonlinear water-wave groups. *Physics Fluids* **14**, 3380–3390.

SJØ, E. 2000 Crossings and maxima in Gaussian fields and sea. *PhD thesis Lund University, Center for Mathematical Sciences.*

SROKOSZ, M. A. & LONGUET-HIGGINS, M. S. 1986 On the skewness of sea-surface elevation. *J. Fluid Mech.* **164**, 487–497.

SKOURUP, J., ANDREASEN, K. K. & HANSEN, N. E. O. 1996 Non-gaussian extreme waves in the central North Sea. *OMAE*, vol. I, part A *Offshore Technology*. ASME.

STOCKER, J. R. & PEREGRINE, D. H. 1999 The current-modified nonlinear Schrödinger equation. *J. Fluid Mech.* **399**, 335–353.

TAYFUN, M. A. 1980 Narrow-band nonlinear sea waves. *J. Geophys. Res.* **85**, 1548–1552.

TRULSEN, K. & DYSTHE, K. B. 1996 A modified nonlinear Schrödinger equation for broader bandwidth gravity waves on deep water. *Wave Motion* **24**, 281–289.

TRULSEN, K., KLIAKHANDLER, I., DYSTHE, K. B. & VELARDE, M. G. 2000 On weakly nonlinear modulation of waves on deep water. *Phys. Fluids* **10**, 2432–2437.

TRULSEN, K. & STANSBERG, C. T. 2001 Spatial evolution of water surface waves: Numerical simulation and experiment of bichromatic waves. *Proc. ISOFE 2001*, vol. 3, pp. 71–77.

WARREN, S. J., BOLE, J. B. & DRIVER, B. D. 1998 Measured wave crest distributions in central and southern North Sea storms. *Proc. ISOPE Conf. 1998*, 96–102.

WHITHAM, G. B. 1967 Non-linear dispersion of water waves *Proc. R. Soc. Lond.* A **299**, 6–25.

ZAKHAROV, V. E. 1967 Stability of periodic waves of finite amplitude on the surface of deep water. *Zh. Prikl. Mekh. Tekh. Fiz.* **9**, 86–94. (English Transl. 1968 *J. Appl. Mech. Tech. Phys.* **9**, pp. 190–194.)